Ecology, 91(3), 2010, pp. 743–755

The contribution of brown vegetation to vegetation dynamics

Gregory S. Okin[1]

Department of Geography, 1255 Bunche Hall, University of California, Los Angeles, California 90095 USA

Abstract. Indices of vegetation dynamics that include both green vegetation (GV) and non-photosynthetic vegetation (NPV), that is, brown vegetation, were applied to MODIS surface reflectance data from 2000 to 2006 for the southwestern United States. These indices reveal that the cover of NPV, a measure of vegetation brownness and a component of ecosystems worldwide, is highly variable in both space and time in the study region. In the more mesic regions of the study area, the timing of peaks in NPV appears to result from simple senescence of GV at the end of the growing season. In these regions, the amplitude of GV cyclicity dominates the total vegetation signal. In contrast, in arid and semiarid regions, the amplitude of cyclicity of NPV dominates the total vegetation signal, showing the vegetation of these regions to be unexpectedly dynamic. Shrublands of southwestern United States exhibit temporal behavior in which the annual peak in NPV cover precedes the annual peak in GV cover by a few months. Several explanations for this behavior are offered. This study shows the importance of vegetation indices that include NPV, or vegetation brownness, in understanding terrestrial ecosystem dynamics, as well as the response to change for these ecosystems.

Key words: deserts; grasslands; phenology; remote sensing; savannas; shrublands; stress; vegetation dynamics; vegetation, green and/or non-photosynthetic; woodlands.

Introduction

Remote sensing has become a powerful tool for observing the Earth's vegetation. With the availability of high temporal resolution time series of remote sensing data aimed at tracking temporal changes in vegetation, starting with the Advanced Very High Resolution Radiometer (AVHRR), and continuing into the Earth Observing System (EOS) era with daily data from the Moderate Resolution Imaging Spectroradiometer (MODIS), a new understanding of the dynamics of vegetation has become possible.

Several important discoveries have been made possible by remote sensing time series of vegetation over wide areas. Many of these discoveries have shown the impacts of climate change on the Earth's vegetation. For instance, Nicholson et al. (1990) used the normalized difference vegetation index (NDVI) to study variable responses of vegetation to rainfall in the Sahel and East Africa. Also using AVHRR data, Jia et al. (2003, 2004) showed that the Alaskan Arctic has been greening in response to climate warming. Delbart et al. (2006) used AVHRR and Satellite Pour l'Observation de la Terre (SPOT) data to show earlier green-up of boreal forests associated with warming. Young and Harris (2005) analyzed AVHRR data from the non-Arctic in the last two decades of the 20th century, finding that over 30% of the Earth's land surface exhibited an increase in photosynthetic activity during this period. Zhang et al. (2007) showed that the effect of warming on the timing of green-up depends on latitude with earlier green-up experienced at high latitudes and later green-up experienced at mid latitudes.

The vast majority of studies that have used remote sensing time series over large areas, including those cited above, have used vegetation indices, such as the NDVI and the Enhanced Vegetation Index (EVI). These indices quantify the difference in reflectance in the red, where chlorophyll absorption dominates, and the near-infrared (NIR), where light scattering within leaf tissue dominates (Curran 1989). Thus, these indices are sensitive to the amount of green vegetation (GV) in an instantaneous field of view (IFOV), as well as its greenness (chlorophyll content) and turgidity (light scattering).

Not all vegetation is green, however. In arid regions, some species have adapted to the harsh conditions through physiological changes that alter the reflectance of photosynthetic tissue (e.g., Ehleringer 1981). In addition, non-photosynthetic vegetation (NPV) is a crucial component of terrestrial ecosystems, whether it is senescent material that contributes organic carbon to soils, standing dead vegetation that can serve as fire fuel, leaves that have yellowed in response to stress, or living structural tissue.

Thus, the focus on greenness in remote sensing of vegetation dynamics has omitted a critical element of ecosystem structure, function, and dynamics. Although NPV appears in the visible primarily as brown material, the largest differences between NPV and GV actually

Manuscript received 20 February 2009; revised 17 June 2009; accepted 23 June 2009. Corresponding Editor: J. Franklin.

[1] E-mail: okin@ucla.edu

occur in the shortwave infrared (SWIR). The loss of water from tissue reduces the dominance of water absorption features in the SWIR, uncovering the absorption features of cellulose and lignin (Curran 1989). Until the launch of MODIS, high temporal resolution data in the SWIR was not available, meaning that understanding the dynamics of NPV did not become feasible until 2000, although earlier work by Roberts et al. (1993), Okin et al. (2001), and Asner and Heidebrecht (2002) have set the stage for quantitative remote sensing of NPV dynamics.

The remote sensing of NPV is further complicated by the similarity between the reflectance of many soils and the reflectance of NPV, particularly when broad wavebands like those used in multispectral sensors are considered. Okin (2007) presented a method, called relative spectral mixture analysis (RSMA), that minimizes the interference of soil in identifying changes in NPV cover and provides indices of both NPV and GV dynamics.

The purpose of this study is to examine, for the first time, the annual dynamics of terrestrial ecosystems, in terms of both vegetation greenness (GV) and vegetation brownness (NPV), in the southwestern United States. It is anticipated that including an index of NPV dynamics, in addition to GV dynamics, considerably enriches the picture that remote sensing can provide about the structure and dynamics of the Earth's ecosystems.

Methods

Derivation of indices of GV and NPV dynamics

RSMA (Okin 2007) was used to create time series of GV and NPV change indices (X_{GV} and X_{NPV}) for two MODIS tiles, h08v05 and h09v05 (Figs. 1, 2). Time series were created using the MODIS 1-km 16-d nadir BRDF-adjusted reflectance (NBAR) product (MOD43B4) from 2000 to 2006. All available MOD43B4 products for this period were used, resulting in a time series for every pixel with 158 separate dates. The study area encompasses much of the arid southwestern United States and northern Mexico. The study period is one of relatively dry conditions in the area, as shown by the average Palmer Drought Severity Index for the region (PDSI; Fig. 1), which could possibly mean that NPV dynamics are greater than would be observed during more mesic periods.

The first step in RSMA is to generate a "baseline spectrum" for each pixel in an image. The baseline spectrum is the apparent surface reflectance of a pixel at a reference time, t_0. At a time, t_i, other than the reference time, RSMA indices quantify change in ground cover components (GV, NPV, and snow) relative to the reference time. RSMA indices are calculated by modeling the pixel reflectance at t_i as a linear combination of four endmembers: the baseline spectrum and reference endmembers for GV, NPV, and snow. The least-squares best-fit coefficients of the GV, NPV, and snow reference endmembers are the RSMA indices X_{GV}, X_{NPV}, and X_{snow}, respectively. For each pixel, time series for the GV and NPV RSMA indices were adjusted by subtracting the mean, thus resulting in time series in which positive values indicate cover greater than the mean for the period 2000–2006, and negative values indicated cover less than the mean for this period.

For each pixel, the mean-adjusted GV and NPV RSMA time series were fit by a cosine function:

$$X_i = A_i \cos(\omega_{date} + \phi_i) + \varepsilon \quad (1)$$

where X_i is the mean-adjusted RSMA time series for the case where i is GV or NPV, A_i is the amplitude of the best-fit cosine to the time series, φ is the phase, and ε is the error of the fit. ω_{date} is the day of the year (DOY) of the last day of the 16-d composite period converted to radians using

$$\omega_{date} = 2\pi\left(\text{year} - 2000 + \frac{\text{DOY}}{365}\right). \quad (2)$$

The best-fit values of A_i and φ_i were determined using the Levenberg-Marquardt algorithm, which combines the steepest descent and inverse Hessian function-fitting methods (Press et al. 1992). Tests using a fast Fourier transform approach show that the two methods provide very similar results.

The use of a cosine function to fit the phenological variables is a way to reduce the dimensionality of the remote sensing data and to create indices that can be easily interpreted. Nonetheless, there are marked drawbacks to the use of a single cosine curve to model the annual cyclicity of vegetation. This approach does not allow identification of double peaks in regions, such as the Sonoran and Chihuahuan Deserts, where vegetation can respond to both winter and summer monsoonal precipitation. In cases such as these, the cosine-fitting algorithm will tend toward the strongest annual cycle, which, at least in terms of GV, is often the summer vegetation peak (Peters and Eve 1995).

Three metrics of vegetation dynamics were derived by combining best-fit values of A_i and φ_i for GV and NPV (Table 1). The first, A_{TV}, is calculated as the sum of A_{GV} and A_{NPV}. A_{TV} provides an index of the total amount of cyclic intraannual variability in a pixel in both GV and NPV. The second metric, A_{NPV}/A_{TV}, is calculated as the ratio of A_{NPV} to A_{TV}. This index describes the fraction of the total cyclic intraannual variability that is due to cyclic changes in NPV. Together, A_{TV} and A_{NPV}/A_{TV} provide information on the amount of cyclic variability that exists in a pixel, and what fraction of that is explained by cyclic variability of NPV.

A third index of vegetation dynamics provides information about the timing of cyclicity of GV and NPV. This index, $\varphi_{GV} - \varphi_{NPV}$, is calculated as the difference between the phases (φ) of GV and NPV. Values of $\varphi_{GV} - \varphi_{NPV}$ near 0.0 or 1.0 indicate that GV and NPV are nearly in phase and thus correlated. Values of $\varphi_{GV} - \varphi_{NPV}$ near 0.5 indicate that GV and NPV are

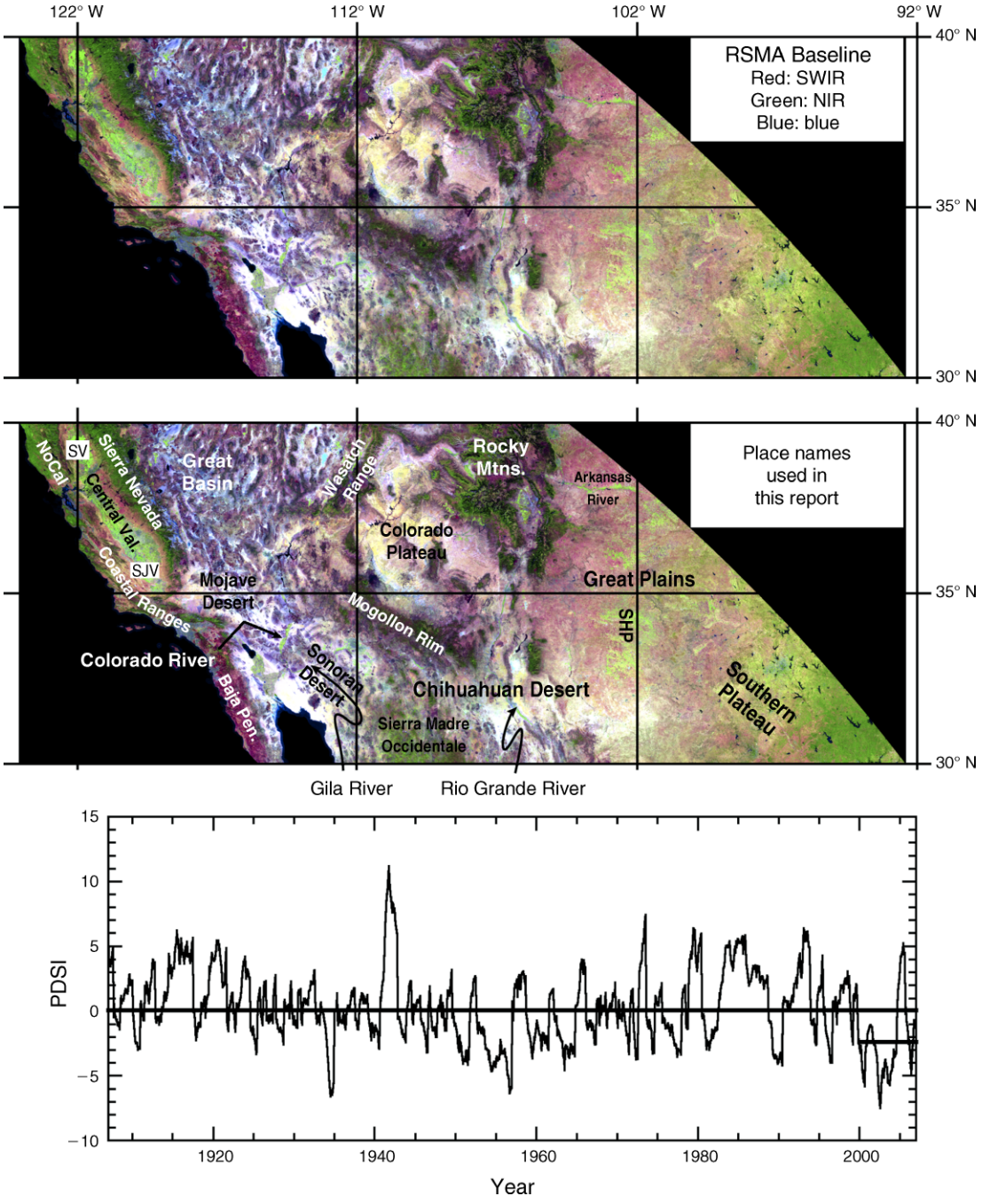

FIG. 1. Top: Baseline image for relative spectral mixture analysis (RSMA) that includes the two MODIS (Moderate Resolution Imaging Spectroradiometer) tiles h08v05 and h09v05. In this image, red is MODIS band 6 (shortwave infrared, SWIR), green is MODIS band 2 (near infrared, NIR), and blue is MODIS band 3 (blue). Middle: The same image with place names from the text overlain. Abbreviations: NoCal, Mountains of Northern California; SV, Sacramento Valley; SJV, San Joaquin Valley; and SHP, Southern High Plains. Bottom: Palmer Drought Severity Index (PDSI) for the southwestern United States showing somewhat dry conditions over the study period. The solid horizontal line through the entire plot is the long-term PDSI average (0.045). The horizontal line on the far right side of the plot is the PDSI average for the period of this study (−2.40). Data are from the National Climate Data Center: ⟨http://www7.ncdc.noaa.gov/CDO/CDODivisionalSelect.jsp⟩.

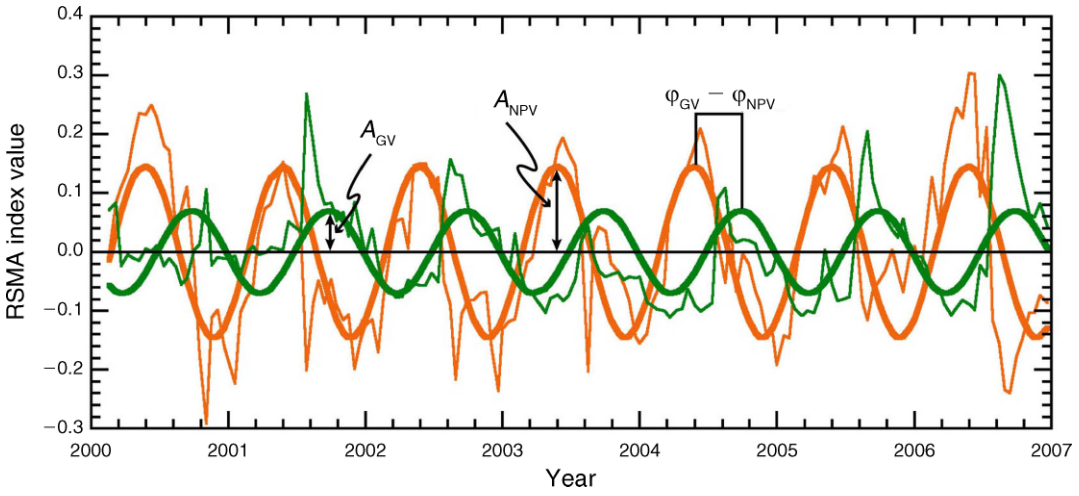

FIG. 2. Time series of RSMA-derived indices of green vegetation (GV) and non-photosynthetic vegetation (NPV) cover (X_{GV} in green and X_{NPV} in orange) minus their respective means for the period 2000–2007. Thin lines show the calculated value of the indices. Thick lines show the best-fit cosine curve to each time series. The best-fit amplitudes of the GV and NPV time series (A_{GV} and A_{NPV}, respectively) are shown along with the difference between their phases ($\varphi_{GV} - \varphi_{NPV}$), which is used to quantify the lag between GV and NPV.

nearly antiphasal and thus anticorrelated. Values of $\varphi_{GV} - \varphi_{NPV}$ that are greater than 0.0 and less than 0.5 indicate that GV peaks before NPV. Values of $\varphi_{GV} - \varphi_{NPV}$ that are greater than 0.5 and less than 1.0 indicate that the peak of NPV precedes that of GV. Of course, difficulties in fitting cosine functions to RSMA time series means that some flexibility is required in interpreting values of $\varphi_{GV} - \varphi_{NPV}$. In practice, values of $\varphi_{GV} - \varphi_{NPV}$ less than 0.1 or greater than 0.9 are interpreted as meaning that GV and NPV are in phase/correlated. Values of $\varphi_{GV} - \varphi_{NPV}$ greater than 0.4 and less than 0.6 are interpreted as meaning that GV and NPV are antiphasal/anticorrelated. Values of $\varphi_{GV} - \varphi_{NPV}$ between 0.1 and 0.4 indicates that the peak of GV leads NPV, whereas values of $\varphi_{GV} - \varphi_{NPV}$ between 0.6 and 0.9 indicates that the peak of NPV leads that of GV.

Comparison between land cover classes and indices of GV and NPV dynamics

Maps of International Geosphere–Biosphere Programme (IGBP) biomes from the MODIS Land Cover product (MOD12C1 from 1 January 2004) were co-registered with maps of vegetation dynamics based on RSMA.

Based on its values of A_{TV}, A_{NPV}/A_{TV}, and $\varphi_{GV} - \varphi_{NPV}$, each pixel was placed into one of three or four categories based on the actual values of each index of vegetation dynamics. These categories are given in Table 1. For each IGBP class present in the study site, the

TABLE 1. Classification criteria and classes for total green vegetation (GV) and non-photosynthetic vegetation (NPV) time-series data.

Total amplitude (A_{TV})			
Low	Medium		High
$A_{TV} < E[A_{TV}] - \sigma(A_{TV})/2$	$A_{TV} \geq E[A_{TV}] - \sigma(A_{TV})/2$ and $A_{TV} < E[A_{TV}] + \sigma(A_{TV})/2$		$A_{TV} \geq E[A_{TV}] + \sigma(A_{TV})/2$
Fraction of total amplitude described by A_{NPV}			
Low	Medium		High
$A_{NPV}/A_{TV} < 0.33$	$A_{NPV}/A_{TV} \geq 0.33$ and $A_{NPV}/A_{TV} < 0.66$		$A_{NPV}/A_{TV} \geq 0.66$
Correlation of GV with NPV ($\varphi_{GV} - \varphi_{NPV}$)			
GV, NPV correlated	GV leads NPV	GV, NPV anticorrelated	NPV leads GV
$\varphi_{GV} - \varphi_{NPV} < 0.1$ or $\varphi_{GV} - \varphi_{NPV} > 0.9$	$\varphi_{GV} - \varphi_{NPV} \geq 0.1$ and $\varphi_{GV} - \varphi_{NPV} \leq 0.4$	$\varphi_{GV} - \varphi_{NPV} > 0.4$ and $\varphi_{GV} - \varphi_{NPV} < 0.6$	$\varphi_{GV} - \varphi_{NPV} \geq 0.6$ and $\varphi_{GV} - \varphi_{NPV} \leq 0.9$

Notes: A is the amplitude; E stands for the expected value, or mean; σ is the standard deviation; and φ is the phase. A_{TV}, is calculated as the sum of A_{GV} and A_{NPV}.

TABLE 2. Relationship between classes as defined using green vegetation (GV) and non-photosynthetic vegetation (NPV) dynamics with IGBP land cover classes from MODIS.

	Three metrics of vegetation dynamics									
	Total amplitude (A_{TV})			Fraction of total amplitude described by A_{NPV} (A_{NPV}/A_{TV})			Correlation of GV with NPV ($\varphi_{GV} - \varphi_{NPV}$)			
IGBP class	Low	Med	High	Low	Med	High	GV, NPV correlated	GV leads	GV, NPV anticorrelated	NPV leads
Evergreen needleleaf forest	70.4	23.1	6.4	32.7	30.6	36.6	11.1	34.8	42.9	11.1
Evergreen broadleaf forest	2.0	19.8	78.2	99.7	0.3	0.0	0.0	6.7	93.2	0.0
Mixed forests	10.3	20.0	69.7	89.6	9.7	0.7	0.1	26.9	73.0	0.1
Closed shrublands	79.2	20.2	0.6	0.7	20.7	78.6	25.3	29.7	5.1	39.9
Open shrublands	25.7	49.2	25.0	1.2	16.8	82.0	17.2	23.5	2.9	56.5
Woody savannas	36.8	35.5	27.6	36.5	37.3	26.2	6.0	26.5	56.8	10.7
Savannas	6.2	38.9	54.8	7.4	46.3	46.3	2.0	10.2	53.4	34.4
Grasslands	27.4	49.2	23.3	22.6	41.8	35.6	7.4	47.1	31.3	14.2
Croplands	6.4	33.6	60.0	55.2	35.7	9.1	1.0	31.3	61.2	6.4
Urban and built up	61.9	24.3	13.8	26.9	30.4	42.7	6.5	20.7	52.1	20.6

Notes: Numbers represent the percentage of the pixels in each International Geosphere–Biosphere Programme (IGBP) class that falls in the classes defined using GV and NPV dynamics. MODIS stands for Moderate Resolution Imaging Spectroradiometer.

percentage of pixels belonging to the RSMA-derived classes was calculated. In addition, a map of World Wildlife Federation (WWF) biomes and ecoregions was co-registered with maps of vegetation dynamics based on RSMA retrievals of GV and NPV (Olson et al. 2001). Using the Zonal Statistics tool in ArcGIS 9 (ESRI 2009), we calculated the median value of A_{TV}, A_{NPV}/A_{TV}, and $\varphi_{GV} - \varphi_{NPV}$ in each biome and ecoregion.

RESULTS

In general, patterns of A_{GV} appear to be closely related to aridity (Fig. 3, top panel). The more arid regions of the study areas (such as the Great Basin, Colorado Plateau, and the Mojave, Sonoran, and Chihuahuan Deserts) regions tend to have lower values of A_{GV}, though there is not a direct correspondence between aridity and A_{GV}. The three indices of vegetation dynamics that include NPV (A_{TV}, A_{NPV}/A_{TV}, and $\varphi_{GV} - \varphi_{NPV}$; Fig. 3) present a starkly different picture than that derived from GV dynamics alone (Fig. 3, top panel). The Colorado Plateau exhibits considerably higher values of A_{TV} than A_{GV}, as do the Mojave, Sonora, and Chihuahuan Deserts. Some regions of the Great Basin also exhibit higher A_{TV} than A_{GV}. The areas of the Great Plains that are in the study area show increased A_{TV} relative to A_{GV}, but the patterns of A_{TV} are similar to those of A_{GV} on the Southern Plateau.

Values of $\varphi_{GV} - \varphi_{NPV}$ provide information about the relative timing of peaks in X_{GV} and X_{NPV}, as delineated in Table 1. In the study area, values of $\varphi_{GV} - \varphi_{NPV}$ span the entire possible range, showing that GV and NPV do not operate simply as mirror images of one another (anticorrelated) nor with the NPV simply following the GV peak. In the most arid regions of the study region, the peak in NPV either precedes or occurs at the same time as the peak in GV.

The percentage of each IGBP class derived from MODIS imagery (1 January 2004; Fig. 4) that occurs in each class based on A_{TV}, A_{NPV}/A_{TV}, and $\varphi_{GV} - \varphi_{NPV}$ (Table 2) shows considerable differences amongst IGBP biomes in terms of the temporal behavior of GV and NPV that they display. Median A_{TV}, median A_{NPV}/A_{TV}, and mode $\varphi_{GV} - \varphi_{NPV}$ calculated for WWF biomes (Fig. 4) further show that the biomes occupy different regions in this three-dimensional data space (Fig. 5).

A more detailed discussion of the results of this study can be found in Appendix A.

DISCUSSION

To date, it has not been possible to observe the simultaneous dynamics of green vegetation (GV) and non-photosynthetic vegetation (NPV) with remote sensing data. The view of phenology of terrestrial ecosystems based on remote sensing has been limited to, and largely shaped by, the availability of indices of GV such as normalized difference vegetation index (NDVI) or enhanced vegetation index (EVI). With the advent of relative spectral mixture analysis (RSMA), the temporal dynamics in NPV have, for the first time, become apparent. Inclusion of NPV with GV when considering temporal dynamics adds considerable depth to the perspective on terrestrial ecosystems provided by remote sensing, and raises several critical questions about how specific biomes function.

First, comparison of the images of A_{GV} and A_{TV} in Fig. 3 shows that the total vegetation dynamics (e.g., NPV and GV) are very different than dynamics that are observable only through estimation of GV cover alone. The A_{GV} image was produced using the RSMA GV index, but NDVI or EVI would have produced very similar results, except in areas with significant snowfall, where these indices perform poorly due to the brightness and low to negative NDVI of snow (Okin 2007).

The simplest interpretation of the A_{GV} image corresponds to common perceptions of deserts; namely, that these ecosystems are vegetatively simple and are characterized by little change from season to season.

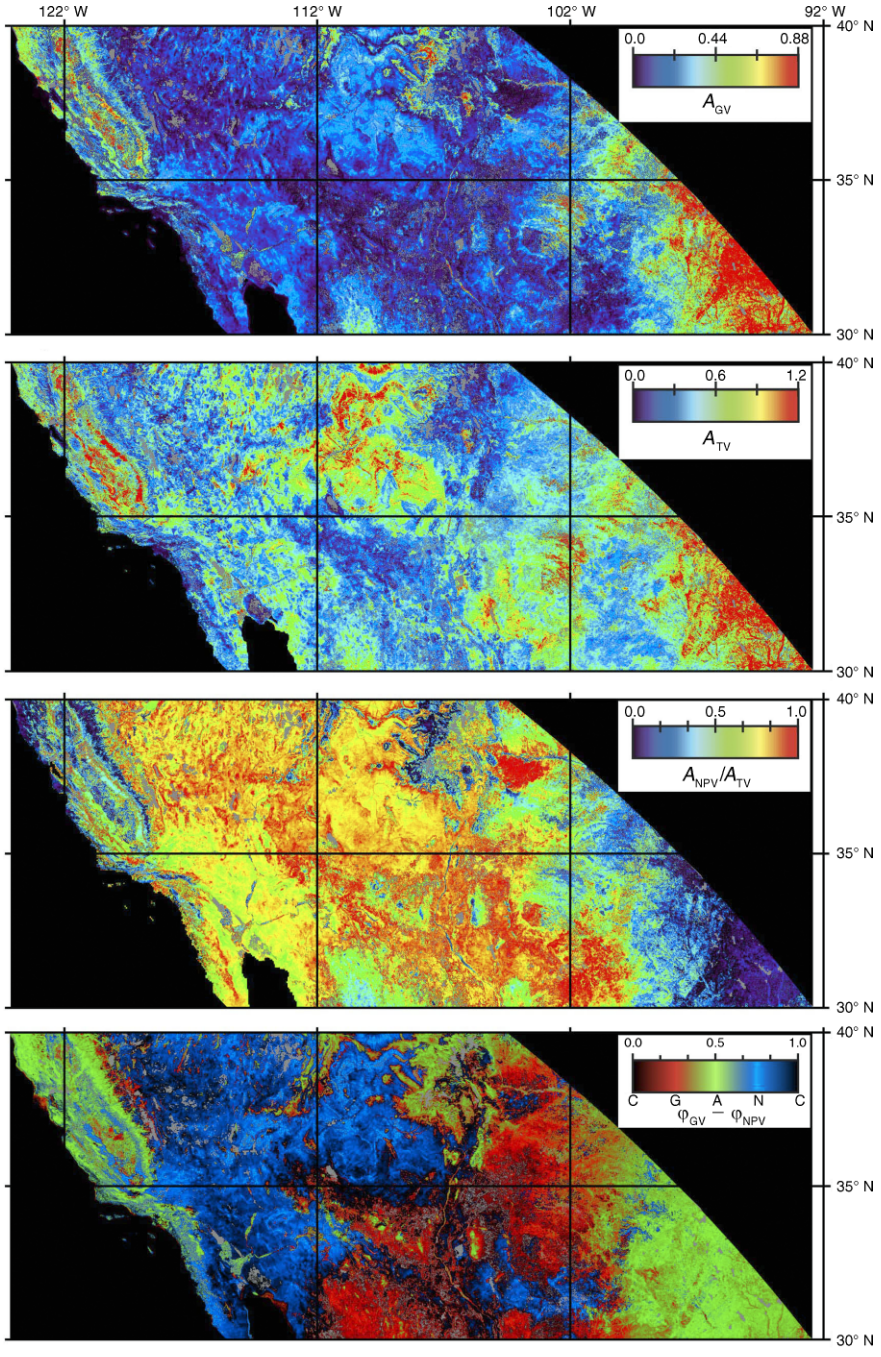

FIG. 3. Four views of vegetation dynamics in the western United States derived from RSMA that includes only GV (top panel) and that includes both GV and NPV (bottom three panels). Gray areas are those where indices could not be calculated due to either high surface reflectance (e.g. playas and permanent snow) or lack of observable vegetation cyclicity resulting in failure of the cosine-fitting routine to converge on a best-fit solution.

While this does appear to be the case in the driest valleys of the Great Basin and a few other isolated spots, the image of A_{TV} shows that for large areas of the arid Southwest, the amplitude of changes in vegetation cover is surprisingly high, rivaling values observed on the more humid Southern Plateau. The high values of A_{TV} on the Colorado Plateau, in particular, are dramatic evidence that concentration solely on GV dynamics presents a rather limited view of ecosystem dynamics.

There are several possible explanations for the large cyclicity observed in NPV cover in the study region (i.e., the high values of A_{NPV}/A_{TV}) though different

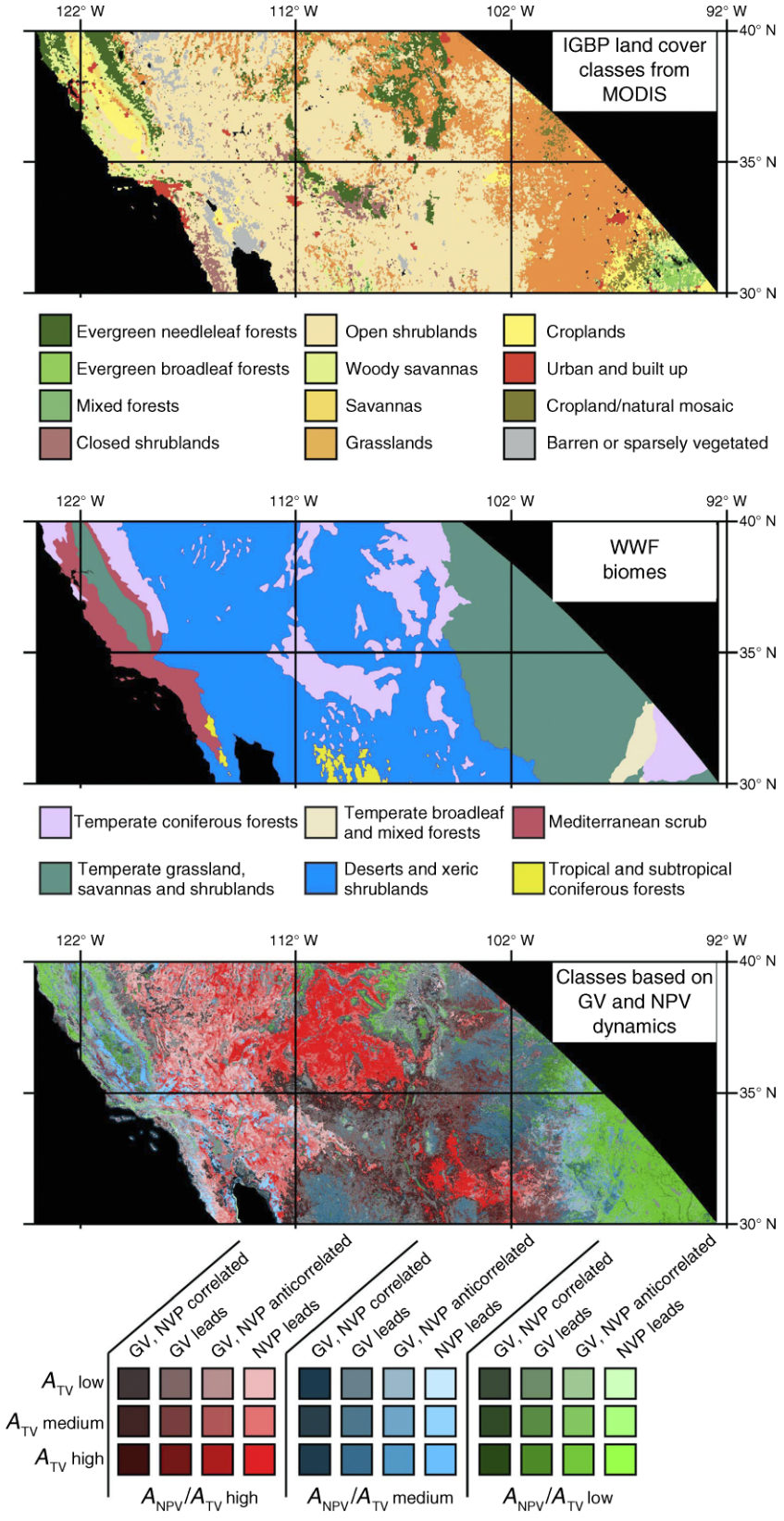

FIG. 4. MODIS-derived IGBP (International Geosphere–Biosphere Programme) land cover classes (top panel), World Wildlife Federation biomes (middle panel; Olson et al. 2001), and vegetation dynamic classes based on GV and NPV (bottom panel). In the bottom panel, gray areas are the same as in Fig. 3. Also see Appendix B.

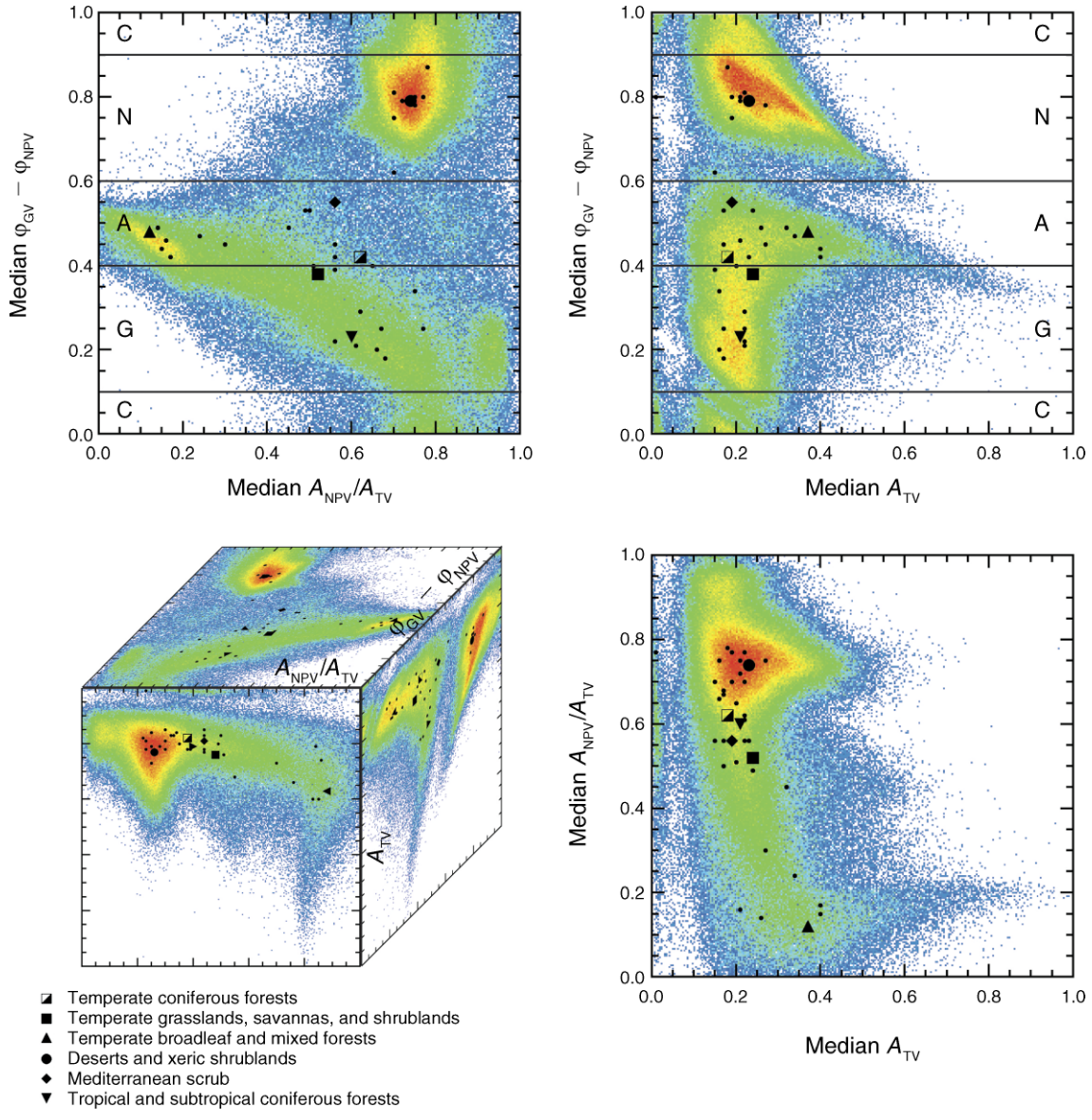

FIG. 5. Scatterplots of all combinations of median A_{TV}, A_{NPV}/A_{TV}, and $\varphi_{GV} - \varphi_{NPV}$ for the entire study area. Colors represent frequency (red is most common, purple is least common). Large symbols (in key) are median values for each biome in the study area. Small dots represent the median values for each of the 31 ecoregions found within the study zone. Several ecoregions are contained within one biome type. The image at the bottom left represents the other three panels projected onto the surface of a cube, with the origin in the middle. The labels C, N, A, and G refer to the phase classes as defined in Table 1 and stand for correlated, non-photosynthetic vegetation (NPV) leads, anticorrelated, and green vegetation (GV) leads, respectively.

explanations may apply in different areas. First, NPV might be caused by standing senescent biomass or litter at the end of the growing season. Second, physical and chemical characteristics of arid-region vegetation (e.g., leaf hairs, low chlorophyll content, and thick waxy cuticles) can lead to spectral signatures that are intermediate between NPV and GV (Okin et al. 2001, Okin and Roberts 2004); thus changes in the cover of this type of vegetation could lead to apparent temporal variability of NPV. Third, the intraannual variability in NPV cover may result from the dominance of NPV-like flowering and fruiting bodies, particularly in grasses during some portions of the year. Fourth, the growth of grasses, which comprise much of the understory vegetation throughout the region, occurs at intercalary meristems, which may cause senescent material, or NPV-like flowering/fruiting bodies in the canopy to spread out resulting in an apparent increase in the cover of NPV. Fifth, spectral changes that accompany annual water stress (Dennison et al. 2003, Camacho-De Coca et al. 2004, Peguero-Pina et al. 2008) could account

for an increase in X_{NPV}, leading to significant values of A_{NPV} in areas where stress occurs annually.

Perhaps the biggest surprise presented by this analysis is that the relative timing of GV and NPV peaks is highly variable. The difference in phase between GV and NPV, captured by $\varphi_{GV} - \varphi_{NPV}$ and shown in Fig. 3, spans the full range from 0.0 to 1.0 years. The case where the GV peak precedes the NPV peak indicates cases where growth in GV is followed about three months later by senescence (a phase difference of 0.25 years or three months). Senescence leads to a decrease in the GV signal and a corresponding increase in the NPV signal. The NPV signal then decreases and there is a period (depending on the site) in which both the NPV and GV signals are low and the spectrum is dominated by the signal of bare ground or snow (not shown).

In the study area, the grasslands of the high plains exhibit this behavior, as do the grasslands of the Owens Valley, which lies on the eastern side of the Sierra Nevada, and a few isolated patches throughout the West. This behavior is entirely consistent with the ecology of these areas, which experience greening during the summer, followed by senescence in the fall, and then a dormant period until the following summer. However, other areas also exhibit this behavior, and the ecological explanation for this change is not entirely clear.

For instance, the GV peak precedes the NPV peak in the evergreen forests of the Mogollon Rim. Here, this behavior is consistent with annual changes in the understory vegetation in an evergreen needleleaf forest. In this forest, both A_{GV} and A_{TV} are low, consistent with the dominance of evergreen species. A_{NPV}/A_{TV} is also low compared to surrounding deserts, indicating a small contribution from the understory. The fact that the small contribution of NPV follows an equally small contribution of GV is thus consistent with dynamics, similar to those of grasslands, of an herbaceous understory. However, the timing of the creation of new needles (with high GV signature) and the senescence of old needles (with high NPV signature) could also explain these dynamics.

Several areas in the study region indicate antiphasal relationships between GV and NPV. The most prominent of these occurs in the western corner of the study area, the Southern Plateau. Here, warm temperatures lead to a longer growing season and an offset of the green and senescent seasons by about six months. In the Rocky Mountains, the Wasatch Range, the Sierra Nevada, and the Coastal Ranges, antiphasal relationships are observed at high altitudes, which cannot be explained by longer growing seasons. Nonetheless, the antiphasal relationship between GV and NPV in these environments is still consistent with typical views of ecosystem timing; namely, the separation of the green and senescent seasons in a way that the senescent season (here, 0.5 year or six months) can follow the green season.

Nearly half of the study area displays values of $\varphi_{GV} - \varphi_{NPV}$ that show GV and NPV to be either in phase with one another (black in Fig. 3) or in a situation where the NPV peak actually precedes the GV peak (blue in Fig. 3). These two cases occur in shrublands of the Great Basin, the Sonoran Desert, the Mojave Desert, and the southern Chihuahuan Desert, as well as the piñon–juniper forests of the Colorado Plateau (cf. Fig. 5).

Neither of these behaviors can be explained simply as senescence following greening. In the case where GV and NPV are in phase, both peak at the same time. This may be due to the growth of new biomass that has spectral characteristics intermediate to GV and NPV. Okin et al. (2001) and Okin and Roberts (2004) showed that some species of desert shrubs have spectral characteristics that are best described as a mixture between GV and NPV. Certainly, species in the genus *Artemesia* (sagebrush), *Atriplex* (saltbush), and *Ambrosia* (bursage and ragweed) are, to the naked eye, neither green nor brown and appear as a mixture between the two. These species are common in the areas that display in-phase relationships between GV and NPV.

In the case where NPV leads GV, this explanation cannot hold. In these areas, NPV peaks, on average, three months prior to the peak in GV. Alternatively, one could say, with equal validity, that the NPV peak follows the GV peak by, on average, nine months. In this alternative phrasing, it could be imagined that the senescent season simply occurs nine months after the green season. However, examination of Fig. 2, which is an example of this behavior, shows this explanation to be untenable. This behavior requires that the GV peak be followed by a period in which both GV and NPV are near their lowest values. If this behavior were simply a result of a long, delayed senescent period, the period of low GV and low NPV couldn't occur.

In the RSMA technique used here, the surface reflectance is modeled as a linear combination of a GV spectrum, an NPV spectrum, a snow spectrum, and a baseline spectrum, which captures any spectral signature of the underlying soil as well as the vegetation present at the reference time. Thus, it might be possible that snow cover accounts for the low vegetation cover (GV + NPV) after the GV peak in areas where $\varphi_{GV} - \varphi_{NPV}$ is near 0.75 (i.e., for areas where the NPV peak leads the GV peak by about three months). Analysis of the amplitude of snow cover cyclicity (A_{snow}, calculated by fitting the RSMA snow cover index to Eq. 2) in Fig. 6, however, shows that snow cover during the low vegetation cover period cannot explain its behavior. A_{snow} has values very close to zero for the majority of areas that show values of $\varphi_{GV} - \varphi_{NPV}$ near 0.75. For the hot deserts of the Southwest, as well as the southern Great Basin, there is practically no snow.

What, then, might lead to the existence of large areas of the southwestern United States in which the apparent peak in NPV cover occurs before the apparent peak in GV cover? In areas with significant grass cover, this

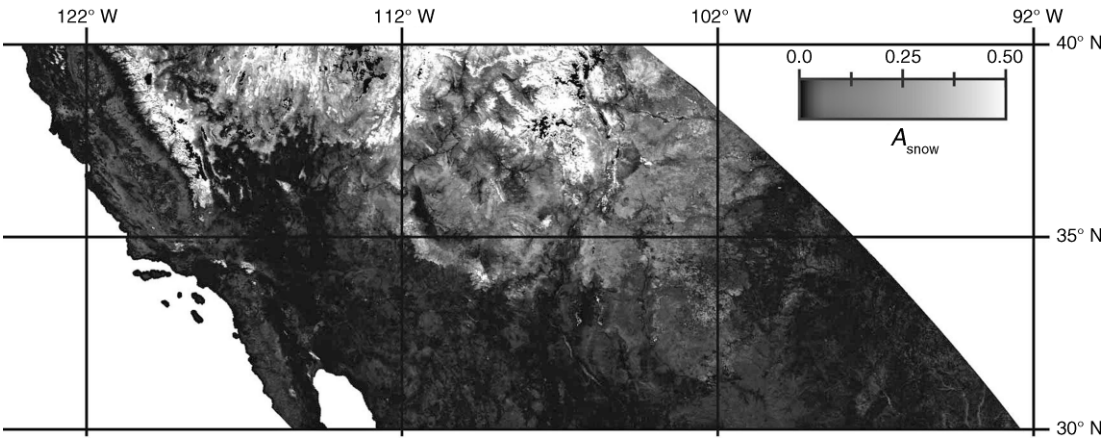

FIG. 6. The amplitude of snow cyclicity, A_{snow}, from relative spectral mixture analysis (RSMA) in the southwestern United States. A_{snow} is calculated by fitting the RSMA snow index time series for each pixel to Eq. 2.

behavior might arise from mechanisms invoked above as possible explanations for high A_{NPV}/A_{TV}; namely, (1) the growth of grasses at intercalary meristems, causing the spreading of non-photosynthetic biomass near the top of the plant, resulting in the appearance of higher canopy cover, or (2) the appearance of flowering or fruiting bodies at the top of the canopy that are spectrally similar to NPV. Of these two possibilities, the first, on the basis of timing, is more likely. The growth at nodes can cause senescent biomass from previous years to spread, causing higher canopy cover. Later in the growing season, the new, green biomass will become increasingly visible through the aging senescent material, so its spectral contribution will increase, causing a peak in the RSMA GV index. Fruiting and flowering bodies in grasses, on the other hand, appear relatively late in the season, and therefore any masking of a GV signal from the grass that they may cause would have to occur later in the season. Neither explanation can account for NPV leading GV in environments without considerable grass cover, such as the Mojave and Sonoran Deserts.

An alternate explanation could arise from the existence of two wet seasons in some portions of the study area. The Chihuahuan and Sonoran Deserts, for instance, have wet seasons during the winter, when precipitation can fall as either rain or snow, and during the summer monsoon. Peters and Eve (1995) have shown that two NDVI peaks occur in the Chihuahuan Desert, though the peak occurring during the summer is stronger. It is possible that the behavior in which the NPV peak leads the GV peak might result from differential responses to the winter and summer wet seasons. Namely, NPV-leading behavior could result (1) if the NPV peak is larger in the winter than the summer (that is, the NPV spectral signature is dominant in response to winter precipitation, but not summer precipitation) and (2) if the GV peak is larger in the summer than the winter (that is, the GV spectral signature is dominant in response to summer precipitation, but not winter precipitation). Nonetheless, the NPV-leading behavior occurs in regions where there is only one wet season, such as the Great Basin and Colorado Plateau. Furthermore, although the Sonoran Desert does have two wet seasons, and exhibits NPV-leading behavior, most of the Chihuahuan Desert, which also has two wet seasons, exhibits in-phase or GV-leading behavior.

Indeed, the region in which the NPV peak precedes the GV peak corresponds to semiarid areas dominated by woody vegetation. In the Mojave and Sonoran Deserts, as well as the Great Basin, this vegetation consists primarily of evergreen shrubs (e.g., creosote, sagebrush). On the Colorado Plateau, the woody vegetation is dominated by trees, such as piñon pine and juniper. Thus, a mechanistic explanation for this behavior might be best aimed at understanding seasonal spectral response of evergreen woody vegetation. Seasonal cycles of precipitation and temperature in these regions cause considerable stress to the vegetation in the hot months before the arrival of rainfall. In areas influenced by the summer monsoon, this stress occurs in the spring, when temperatures have increased but summer rains have not yet arrived. In areas dominated by winter rainfall, the time of greatest stress occurs in the fall, at the end of a long, dry summer. Thus, in both summer- and winter-rainfall shrublands/woodlands, the period of maximum stress occurs in the season immediately prior to the wet season. This pattern would lead to the peak of the NPV signature occurring in the season prior to the peak in the GV signature, even in areas where the standing biomass does not change cyclically throughout the year.

In the absence of a clear mechanistic explanation for the NPV peak leading the GV peak, it is imperative to determine the likelihood that this is a real observation and not the result of instrument noise or an artifact of

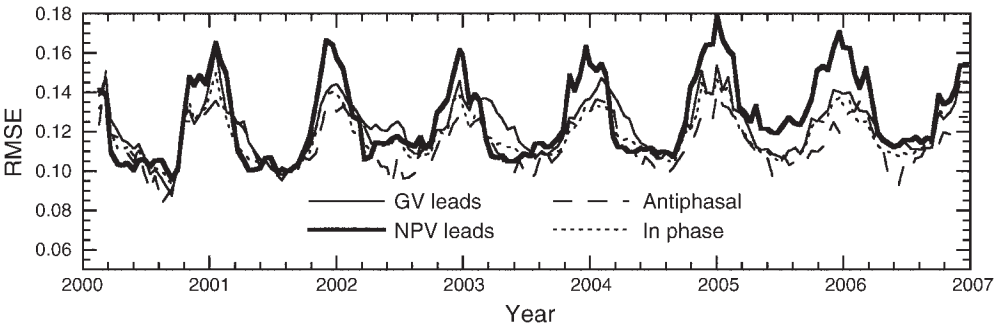

FIG. 7. Time series of average root mean squared error (RMSE) for each of the four types of temporal behavior: GV peak leads NPV peak, NPV peak leads GV peak, GV and NPV are in phase, GV and NPV are antiphasal.

the algorithms. Several critical observations argue that this behavior is real.

1) The large spatial extent and the spatial continuity of the blue areas in Fig. 3 argue that this result is not an artifact created by instrument noise.

2) The boundaries of the blue areas in Fig. 3 correspond to real biome boundaries; the outline of the Great Basin, Colorado Plateau, Mojave Desert, and Sonoran Deserts, as well as the western Chihuahuan Desert are clearly visible. This argues for the correspondence between the observed behavior with real biome dynamics.

3) RSMA is run for each MODIS tile without regard to biome boundaries, and only one endmember of GV and of NPV are used. Therefore, the behavior cannot arise due to geographically related differences in the algorithm or the selection by the algorithm of different GV and NPV endmembers.

4) Visual inspection of time series from individual pixels (such as the one shown in Fig. 2) confirms that the NPV peak actually does occur before the GV peak, meaning that the fitting algorithm does result in adequate fits of the time series to Eq. 2.

5) There is no logical candidate for a ground cover component that could have high cover when GV and NPV have low cover that is not included in RSMA. RSMA includes GV and NPV, or a combination of both, as well as snow. Changes in soil cover are included, though the soil spectrum is not considered explicitly; changes in the apparent cover of soil appear as changes to the RSMA baseline index (Okin 2007). It is possible that a cyclic change in soil moisture could change the underlying soil spectrum in such a way that the NPV RSMA index increased. Any such change would, however, show up as an increase in the root mean squared error (RMSE) of the fit during the NPV peak, and this error would only be found in areas where the NPV peak appears to lead the GV peak. Fig. 7 shows that the average RMSE for all pixels that display NPV-leading behavior appears in the winter, whereas the NPV peak typically occurs during the early summer (Fig. 2). Thus, seasonal changes in soil moisture do not appear to be able to explain NPV-leading behavior. In addition, when the average RMSE for all pixels that display NPV-leading behavior ($\varphi_{GV} - \varphi_{NPV} \sim 0.75$) is compared with the average RMSE for all pixels that display GV-leading behavior ($\varphi_{GV} - \varphi_{NPV} \sim 0.25$), antiphasal behavior ($\varphi_{GV} - \varphi_{NPV} \sim 0.5$), or in phase behavior ($\varphi_{GV} - \varphi_{NPV} \sim 0.0$), all pixels appear to have the same temporal patterns and magnitude of RMSE (Fig. 7). For all four behaviors, the increase during the winter could be explained by changes in lighting conditions discussed by Okin (2007). The similarity of NPV-leading RMSE patterns with those of other pixels also clearly shows that there is not a missing endmember that can somehow explain away the NPV-leads behavior.

A large portion of the study area displays behavior in which the RSMA index of NPV peaks before the GV peak, particularly in the woody deserts of the Southwest. In light of the discussion above, we are forced to conclude that this behavior is real, in the sense that the fractional cover of NPV-like material seen from the zenith peaks during the early summer prior to the peak in GV-like material. Further research is required to determine the actual cause of this behavior, and its exact implications for understanding ecosystem structure and function in arid environments, though a mechanism invoking dry-season stress in woody evergreen vegetation would seem to explain this behavior in the simplest way.

CONCLUSIONS

Nonphotosynthetic vegetation, whether it is structural material, standing dead biomass, fully or partially senesced leaves, or leaf litter, is a crucial element of the structure and function of all terrestrial ecosystems. In addition, the spectra of many plants found in arid and semiarid regions during their growing seasons appear as mixtures of GV and NPV signatures, meaning that the changes in the cover of these plants, or changes in their stress level, appears as changes in the amount of NPV-like material in remote sensing images. Until recently, there has been no way to observe the temporal dynamics of NPV or NPV-like living material, that is to say vegetation brownness, over large areas. This paper presents, for the first time, a large-scale picture of the

dynamics of NPV and NPV-like material in the southwestern United States. This region did experience relatively dry conditions during the study period (Fig. 1). Although this fact may result in the strength of the NPV cyclicity being slightly higher than under usual conditions in some cases, it does not diminish the fact that NPV and NPV-like material have significant contributions to the total vegetation dynamics in the region.

There are two main results from this study that are somewhat surprising. The first is the large magnitude of cyclic variation in NPV throughout much of the study area. When the entire contribution of vegetative materials (GV + NPV) are considered, the amplitude of annual cycles of vegetative cover in the arid regions of the study area rival those of the wetter portions of the study area on the Southern Plateau suitable for agriculture. Throughout much of the study area, the majority of the annual changes in vegetative growth occur as a result in annual changes in NPV.

The second major finding of this study is the relationship between peaks in GV and peaks in NPV, and particularly the case in which the NPV peak occurs prior to the GV peak. This behavior occurs in a spatially contiguous area throughout much of the arid and semiarid Southwest. No mechanistic explanation for this behavior is immediately clear, but one hypothesis would seem most likely: that changes in the apparent cover of NPV due to stress in evergreen woody vegetation lead to the appearance of the NPV peak just prior to the GV peak. Although further research is required to evaluate the exact causes of this NPV-leads behavior, it does appear to be real. Because this behavior characterizes vegetation dynamics throughout much of the study area, we consider its identification to be a major finding of the present research, as well as a potential jumping-off point for future research. The ability to identify stressed woody vegetation in multispectral imagery could be a key tool in the early detection of drought or vegetation dryness that leads to the potential for wildland fires.

In this study, we have shown that the temporal signature of both GV and NPV observed with a Moderate Resolution Imaging Spectroradiometer (MODIS) is highly variable in both space and time. Using vegetation indices, many previous studies have focused on variability in GV and the critical phenological information that they can provide from remote sensing data. Here, we show that there is significant information on ecosystem dynamics, particularly in arid and semiarid regions, to be gained by looking at the temporal signature of NPV as well. Indeed, dry lands in the present study show surprisingly large intraannual variations in the apparent cover of NPV, signifying that these regions are as dynamic as their more humid counterparts. This is a critical observation for the management of the world's dry lands. Dry lands cover about 40% of the Earth's land surface and land degradation in dry lands directly affects some 250 million people in the developing world, an estimate likely to expand substantially in the face of climate change and population growth (Reynolds et al. 2007). The creation of remote sensing tools that can adequately describe the dynamics of vegetation in these regions is crucial for understanding the ecology of these ecosystems as well as contributing to their management.

Acknowledgments

This work was supported by NSF grants DEB-0618210, DEB-0823205, and EAR-072021. The author thanks Susan Ustin and two anonymous reviewers for their helpful comments.

Literature Cited

Asner, G. P., and K. B. Heidebrecht. 2002. Spectral unmixing of vegetation, soil and dry carbon cover in arid regions: comparing multispectral and hyperspectral observations. International Journal of Remote Sensing 23:3939–3958.

Camacho-De Coca, F., F. J. Garcia-Haro, M. A. Gilabert, and J. Melia. 2004. Vegetation cover seasonal changes assessment from TM imagery in a semi-arid landscape. International Journal of Remote Sensing 25:3451–3476.

Curran, P. J. 1989. Remote sensing of foliar chemistry. Remote Sensing of Environment 30:271–278.

Delbart, N., T. Le Toan, L. Kergoat, and V. Fedotova. 2006. Remote sensing of spring phenology in boreal regions: a free of snow-effect method using NOAA-AVHRR and SPOT-VGT data (1982–2004). Remote Sensing of Environment 101:52–62.

Dennison, P. E., D. A. Roberts, S. R. Thorgusen, J. C. Regelbrugge, D. Weise, and C. Lee. 2003. Modeling seasonal changes in live fuel moisture and equivalent water thickness using a cumulative water balance index. Remote Sensing of Environment 88:442–452.

Ehleringer, J. 1981. Leaf absorptances of Mohave and Sonoran Desert plants. Oecologia 49:366–370.

ESRI. 2009. ArcGIS 9. Environmental Systems Research Institute (ESRI), Redlands, California, USA.

Jia, G. S. J., H. E. Epstein, and D. A. Walker. 2003. Greening of arctic Alaska, 1981–2001. Geophysical Research Letters 30:2067.

Jia, G. S. J., H. E. Epstein, and D. A. Walker. 2004. Controls over intra-seasonal dynamics of AVHRR NDVI for the arctic tundra in northern Alaska. International Journal of Remote Sensing 25:1547–1564.

Nicholson, S. E., M. L. Davenport, and A. R. Malo. 1990. A comparison of the vegetation response to rainfall in the Sahel and East Africa using Normalized Difference Vegetation Index from NOAA AVHRR. Climatic Change 17:209–241.

Okin, G. S. 2007. Relative Spectral Mixture Analysis: a multitemporal index of total vegetation cover. Remote Sensing of Environment 106:467–479.

Okin, G. S., W. J. Okin, B. Murray, and D. A. Roberts. 2001. Practical limits on hyperspectral vegetation discrimination in arid and semiarid environments. Remote Sensing of Environment 77:212–225.

Okin, G. S., and D. A. Roberts. 2004. Remote sensing in arid environments: challenges and opportunities. Pages 111–146 *in* S. L. Ustin, editor. Remote sensing for natural resource management and environmental monitoring. John Wiley and Sons, New York, New York, USA.

Olson, D. M., et al. 2001. Terrestrial ecoregions of the worlds: a new map of life on Earth. Bioscience 51:933–938.

Peguero-Pina, J. J., F. Morales, J. Flexas, E. Gil-Pelegrin, and I. Moya. 2008. Photochemistry, remotely sensed physiological reflectance index and de-epoxidation state of the

xanthophyll cycle in *Quercus coccifera* under intense drought. Oecologia 156:1–11.
Peters, A. J., and M. D. Eve. 1995. Satellite monitoring of desert plant community response to moisture availability. Environmental Monitoring and Assessment 37:273–287.
Press, W. H., S. A. Teukolsky, W. T. Vetterling, and B. P. Flannery. 1992. Numerical recipes in C: the art of scientific computing. Second edition. Cambridge University Press, Cambridge, UK.
Reynolds, J. F., et al. 2007. Global desertification: building a science for dryland development. Science 316:847–851.
Roberts, D. A., M. O. Smith, and J. B. Adams. 1993. Green vegetation, non-photosynthetic vegetation, and soils in AVIRIS data. Remote Sensing of Environment 44:255–269.
Young, S. S., and R. Harris. 2005. Changing patterns of global-scale vegetation photosynthesis, 1982–1999. International Journal of Remote Sensing 26:4537–4563.
Zhang, X. Y., D. Tarpley, and J. T. Sullivan. 2007. Diverse responses of vegetation phenology to a warming climate. Geophysical Research Letters 34:L19405.

APPENDIX A

Extended discussion of results with particular emphasis on geographic provinces in the study area (*Ecological Archives* E091-054-A1).

APPENDIX B

Full resolution version of Fig. 4 with annotated version of true-color image including place names (*Ecological Archives* E091-054-A2).